J1.2 ICE CLOUD EFFECTIVE PARTICLE SIZE PARAMETERIZATION DERIVED USING COMBINED LIDAR AND RADAR DATA

D.P. Donovan*
Royal Netherlands Meteorological Institute, De Bilt, the Netherlands

1. INTRODUCTION

An important parameter for determining the radiative characteristics of a cloud is the effective radius ($R_{\rm eff}$) of its consistent particles. For a given cloudly volume, $R_{\rm eff}$ determines the relationship between the total mass and optical depth and influences the associated phase function and single-scattering albedo. For ice particles we may define

$$R_{\rm eff} = \frac{3}{4}\frac{\langle M(D)/\rho_{s,i}\rangle}{\langle A_c(D)\rangle}, \quad (1)$$

where the braces denote averaging over the particle size distribution, D is the particle maximum dimension, M is the mass, A_c is the cross-section area and, $\rho_{s,i}$ is the density of solid ice. This definition preserves the ratio between the total mass (which largely determines the amount of absorption) and the total cross-sectional area (which largely determines the total extinction) (Grenfell and Warren [1999]).

Since the explicit treatment of ice cloud microphysics is beyond the capabilities of large scale atmospheric models, it is necessary to parameterize their microphysical properties. Previous parameterizations of ice cloud R_{eff} have been formulated using observations made in situ using aircraft mounted instrumentation (i.e. Heymsfied and Platt [1984]). In situ approaches more-or-less directly measure the particle size distribution. However, it is difficult to obtain large in situ data sets. In contrast, lidars and radars sample entire cloud profiles instantaneously and may operate continuously for long periods of time. In this paper, we present a long time-series of ice cloud effective size and ice water content (IWC) measurements made using combined lidar and radar observations. The method has been applied to 5 months of data taken at the Atmospheric Radiation Measurement Program's Southern Great Plains (ARM-SGP) site. The relationships between retrieved particle size, IWC and temperature (T) are presented and discussed.

*Corresponding author address: D.P. Donovan, KNMI PO Box 201, 3730 AE, De Bilt, The Netherlands

2. LIDAR/RADAR CLOUD REMOTE SENSING

Lidars and cloud radars are active sensors. That is, they transmit pulses of electomagnetic radiation and detect the backscattered signal as a function of time after the pulses have been launched. Lidars and radars however, operate at very different wavelengths (microns vs millimeters) so they are most sensitive to particles in different size regimes. This difference in sensitivity may be used to estimate an effective size for cloud particles.

2.1 *Relationship between Radar reflectivity (Z_e) and optical extinction*

For non-spherical ice particles, formal scattering calculations can only be carried out for a limited number of idealized cases. However, with respect to Z_e, so long as the cloud particles are 'small' the dominant factor determining their scattering properties is their mass. Further, with respect to the optical extinction, the dominant factor is the particles cross-sectional area. Thus, for the radar reflectivity (Z_e) we have

$$Z_e \propto N_o \left\langle M^2(D)\right\rangle \quad (2)$$

where N_o is the total number of particles and for the optical extinction (α_{lid}), we have

$$\alpha_{lid} \propto No \left\langle A_c D\right\rangle \quad (3)$$

Thus the relationship between Z_e and α_{lid} can be expressed as

$$\frac{Z_e}{\alpha_{lid}} = C R_{eff}^{\prime 4} \quad (4)$$

where C is a known constant and R'_{eff} is the *lidar/radar effective radius* defined as

$$R_{\rm eff}^{\prime 4} = \frac{9}{16\pi\rho_{s,i}^2}\frac{\left\langle M^2(D)\right\rangle}{\langle A_c(D)\rangle} = R_{\rm eff}\frac{3}{4\pi\rho_{s,i}}\frac{\left\langle M^2(D)\right\rangle}{\langle M(D)\rangle}. \quad (5)$$

The Z_e/α_{lid} relationships for size distributions of columns and plates as a function of R'_{eff} are shown in Figure 1. Here it can be seen that there is only a small difference between the values for spheres, columns and plates.

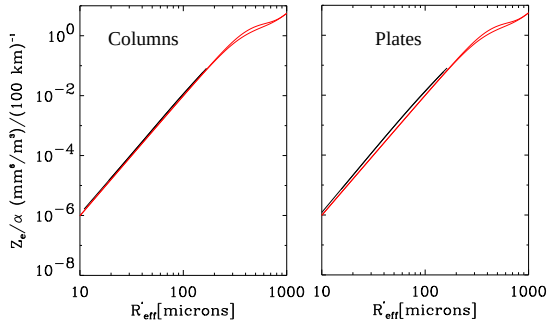

Figure 1: Z_e/α_{lid} for gamma-type size distributions of columns (Left-blank-lines), plates (right-black lines) and spheres (red lines). The different red lines correspond to different size distribution width parameters. The results for the crystals were produced for a lidar wavelength of 532 nm using Raytracing calculations together with a radar frequency of 95 GHz using Discrete Dipole Approximation (DDA) calculations (Lemke and Quante (1999)). The calculations for the spheres were made using Mie theory.

Corresponding to R'_{eff}, the lidar/radar effective ice water content (IWC′) can be estimated using Z_e together with $R'_{\rm eff}$. IWC′ is related to IWC as

$$\mathrm{IWC}' = \mathrm{IWC}(R'_{\rm eff}/R_{\rm eff}). \qquad (6)$$

2.2 Inversion Procedure

Here, a short overview of combined lidar/radar inversion procedure used here is given. A detailed description is given in Donovan et al. (2001).

$R'_{\rm eff}$ can be estimated if the lidar extinction together with the Z_e profiles are known. However, the lidar extinction must first be extracted from the lidar signal which is a function of both the lidar backscatter and extinction and can be written, assuming single scattering, as

$$P_{ss}(z) = C_{\rm lid} z^{-2} \beta_{\rm lid} \exp\left[-2\int_{z_o}^{z} \alpha_{\rm lid}(z')dz'\right], \qquad (7)$$

where z is the altitude, $P_{\rm ss}(z)$ is the returned single scattering power, $\beta_{\rm lid}$ is the backscattering coefficient at the lidar wavelength, and $\alpha_{\rm lid}$ is the corresponding extinction coefficient. Here $C_{\rm lid}$ is the effective calibration constant. A novel procedure for retrieving the extinction from the lidar signal has been developed. This procedure makes use of the previously discussed relationship between Z_e, α_{lid} and R'_{eff}. The procedure has been found to be stable with respect to variations in the cloud backscatter-to-extinction ratio profile as well as measurement errors.

For lidar cloud measurements, multiple scattering can significantly contribute to the observed signal. An approximate treatment of multiple-scattering effects has been incorporated into the inversion process. As described in Donovan et al. (2001), an iterative correction for multiple scattering is used in the inversion procedure.

3. APPLICATION TO ARM DATA

The lidar/radar method was applied to data taken from ARM-SGP site. An example is shown in Figure 2. The data were acquired using the ARM Micro-Pulse Lidar (MPL) operating at 532 nm and the ARM 35-GHz cloud radar (for instrument descriptions consult www.arm.gov).

A total of 5 months of data were examined. The ensemble results are shown in terms of a cumulative density function contour plot in Figure 3. The minimum altitude considered was 4 km. Points where the estimated retrieval error was greater than 30% were not considered. Suspected areas of supercooled water layers (Illingworth et al. [2000]), were encountered above 4 km on roughly 5% of the days examined and were excluded from the analysis. The temperature information was provided by sondes launched up to every four hours from the ARM site. The results show that, in general, that R'_{eff} increases with temperature and that the dependence of R'_{eff} on temperature increases with increasing effective ice-water content.

3.1 Size Distribution Model

Similar to Mitchell et al. (1996), we will consider bimodal generalized gamma distributions of the form

$$\frac{dn}{dr} = \sum_{i=1}^{2} \frac{N_{o,i}}{r_{m,i}} \frac{1}{\Gamma(\gamma_i)} \left(\frac{r}{r_{m,i}}\right)^{(\gamma_i - 1)} exp[-r/r_{m,i}], \qquad (8)$$

where $r = D/2$, $N_{o,i}$ denote the total number of scatterers in each respective mode, γ_i denote the width parameters, and $r_{m,i}$ denote the mode radii.

Once the size distribution parameters along with an ice crystal habit model are specified $R'_{\rm eff}$ (and $R_{\rm eff}$) can be computed. The results produced by fixing all the parameters of the small particle mode (mode 1) and varying $N_{o,2}$ along with $r_{m,2}$ are shown in Figure 4 (left panel). It can be seen that $N_{o,2}$ controls how sensitive the relationship between $R'_{\rm eff}$ and $r_{\rm eff,2}$ is. Associating $r_{m,2}$ with temperature and $N_{o,2}$ with IWC′ closely matches the observed behavior of our data set. Fits of equation (8) to the data were made assuming various crystal habits. In the fits, γ_1 was fixed at 1.0 (following Mitchell et al. (1996)); single "universal" values of γ_2 and $r_{m,1}$ were also used but were treated as

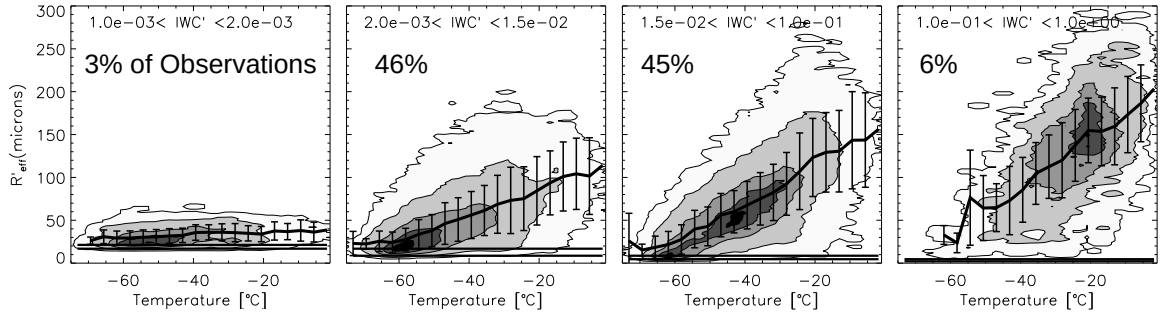

Figure 3: Density plot of the total data set. Each panel corresponds to a range of IWC′(gm^{-3}) values The error bars show the standard deviation while the vertical lines mark the sensitivity limits of the observations for the different IWC′ ranges. The contours correspond to 10,30,60,90 and 99% of the measurements respectively

fitting parameters, $N_{o,2}/N_{o,1}$ was modeled as a polynomial function of IWC′, and $r_{\mathrm{eff},2}$ was treated as a polynomial function of T.

Once the size distribution models have been found, the corresponding translation from R'_{eff} and IWC′ space to R_{eff} and IWC space can be made using equations (5) and (6) in an iterative fashion. Such a procedure can be used to find size distributions corresponding to particular values of IWC and T. Sample size distributions derived from the complex polycrystal fit parameters are shown in the left panel of Figure 5 for two values of IWC and T. Using a similar iterative procedure, the variation of R_{eff} with T for different values of IWC was calculated and is presented in the right panel of Figure 5.

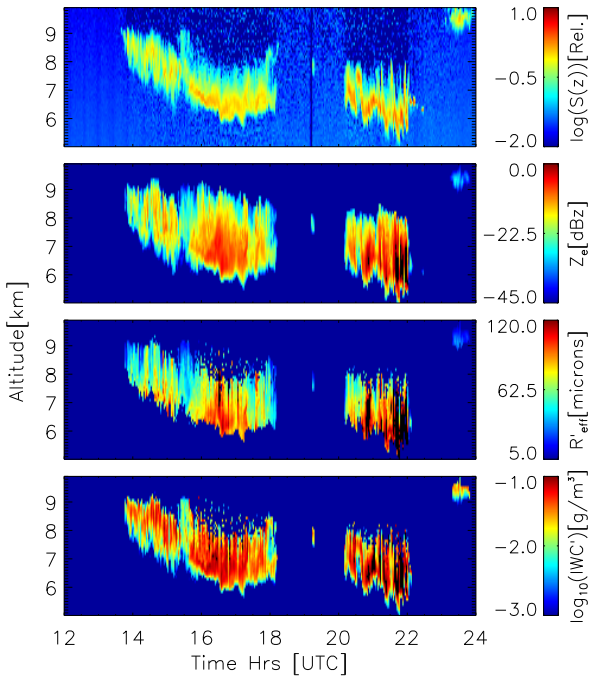

Figure 2: 532-nm lidar signal (top panel), 35-GHz radar reflectivity, as well as derived R'_{eff} and IWC′ (bottom panel) for Jan 10, 2000.

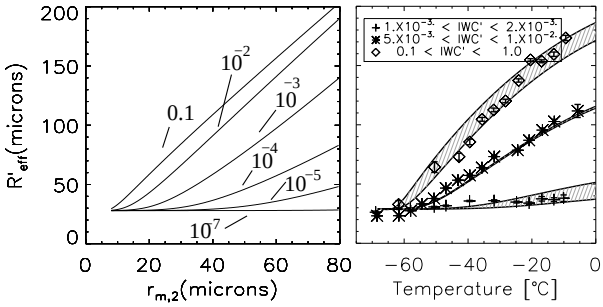

Figure 4: (Left) R'_{eff} as a function of $r_{m,2}$ for various values of $N_{o,2}/N_{o,1}$ (shown as line labels). Here $r_{m,1}$ = 10 μm, γ_1 =1, and γ_2 = 3. (Right) Sample fit results for 3 IWC′ ranges. The shaded areas correspond to minimum and maximum IWC′ limits for the indicated range Here, the complex polycrystal habit was assumed.

4. SUMMARY

The data clearly show that both IWC and temperature influence the average value of R_{eff}. The observed behavior of ice crystal effective size with temperature is broadly consistent with the parameterization adapted by Kristtjansson et al. (2000) and with other studies indicating that R_{eff} tends to increase with increasing IWC and T (Heymsfied and Platt [1984]).

The tendency for ice crystals effective size to increase with temperature has also been noted in data obtained by the inversion of TIROS-N observations. However, the average effective cirrus particle effective size range reported by Stubenraunch et al. (1999) of 26–34 μm is somewhat higher than the average value obtained in this study (15-20 microns).

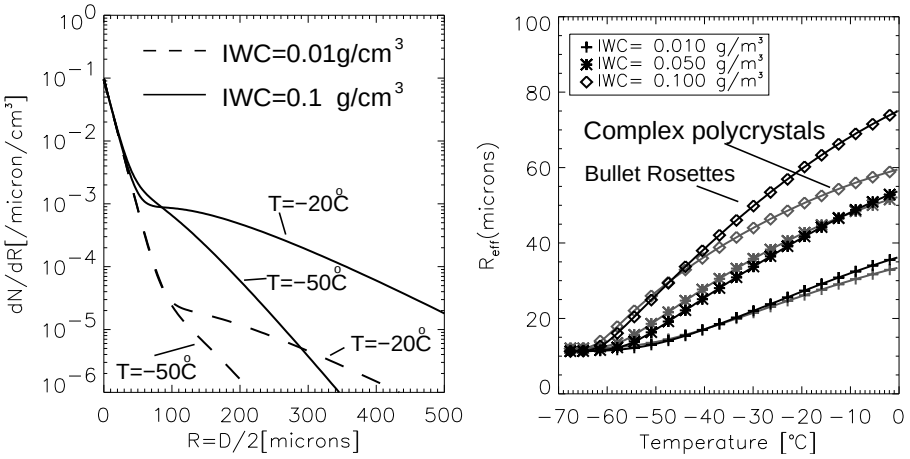

Figure 5: (Left) Sample complex polycrystal model size distributions for two different IWC values and temperatures. The distributions have been normalized to have the same peak value. (Right) Effective radius (R_{eff}) as a function of temperature for different values of IWC for two different crystal habit models.

The significance of this comparison is unclear owing to the different 'viewing geometries' (i.e. the TIROS observations represent some sort of altitude averaged size viewed from space) and sampling strategies. (i.e. the TIROS study considered hemispheric land/ocean averages of large (100x100km) areas of overcast cirrus while the results here are for a few scattered months for a single land site).

Acknowledgments

The contribution of M. Quante (GKSS,Geeshacht Germany) who made the DDA calculations used here available is gratefully acknowledged. The technical support of members of the U.S. ARM program is also gratefully acknowledged.

5. REFERENCES

Donovan et al., 2001: Cloud effective particle size and water content profile retrievals using combined lidar and radar observations, 1. Theory and examples, *J. Geophys. Res.*, *106*, 27,425–27,448.

Heymsfied A. J., and C. M. R. Platt, 1984: A Parameterization of the particle spectrum of ice clouds in terms of the ambient temperature and the ice water content, *J. Atmos. Sci.*, *41*, 846-855.

Illingworth A. et al., 2000: Quantification of synergy aspects of the Earth radiation mission, Tech. Rep. ISSN 1436-5235, ESTEC contract 13167/98/NL/GD, ESA/ESTEC Noordwijk, The Netherlands.

Grenfell, T. C., and S. G. Warren, 1999: Representation of a nonspherical ice particle by a collection of independent spheres for scattering and absorption of radiation, *J. Geophys. Res. 104,* 31,697–31,709.

Kristjánsson, J. E., J. M. Edwards, and D. L. Mitchell,2000: Impact of a new scheme for optical properties of ice crystals on climates of two GCMs, *J. Geophys. Res.*, *105*, 10,063–10,079.

Lemke H.M., and M. Quante, 1999: Backscatter characteristics of nonspherical ice crystals: Assessing the potential of polarimetric radar measurments, *J. Geophys. Res.*, *104*, 31,739–31,751.

Mitchell, D.L., et al., 1996: Modeling cirrus clouds. Part 1: Treatment of bimodal size spectra and case study analysis, *J. Atmos. Sci.*, *53*, 2952–2966.

Stubenraunch C. J., et al.,1999: Retrieval of cirrus crystal sizes from 8.3 and 11.1 μm emissivities determined by the improved initialization inversion of TIROS-N Operational Vertical Sounder observations, *J. Geophys. Res. 104*, 31,793–31,808.